Journal Pre-proof

Localized waves at a line of dynamic inhomogeneities: General considerations and some specific problems

Gennady S. Mishuris, Alexander B. Movchan, Leonid I. Slepyan

PII: S0022-5096(20)30137-X
DOI: https://doi.org/10.1016/j.jmps.2020.103901
Reference: MPS 103901

To appear in: *Journal of the Mechanics and Physics of Solids*

Received date: 24 December 2019
Revised date: 9 February 2020
Accepted date: 9 February 2020

Please cite this article as: Gennady S. Mishuris, Alexander B. Movchan, Leonid I. Slepyan, Localized waves at a line of dynamic inhomogeneities: General considerations and some specific problems, *Journal of the Mechanics and Physics of Solids* (2020), doi: https://doi.org/10.1016/j.jmps.2020.103901

Localized waves at a line of dynamic inhomogeneities: General considerations and some specific problems

Gennady S. Mishuris[a], Alexander B. Movchan[b] and Leonid I. Slepyan[c*]

[a] *Department of Mathematics, IMPACS, Aberystwyth University, SY23 3BZ, Wales, UK*
[b] *Department of Mathematical Sciences, University of Liverpool, Liverpool, L69 7ZL, UK*
[c] *School of Mechanical Engineering, Faculty of Engineering, Tel Aviv University P.O. Box 39040, Ramat Aviv 69978 Tel Aviv, Israel*

* Corresponding author
Email: slepyanl@tauex.tau.ac.il (L.I. Slepyan)

Abstract

We consider a *body*, homogeneous or periodic, equipped with a *structure* composed of dynamic inhomogeneities uniformly distributed along a line, and study free and forced sinusoidal waves (Floquet - Bloch waves for the discrete system) in such a *system*. With no assumption concerning the wave nature, we show that if the structure reduces the phase velocity, the wave localizes exponentially at the structure line, and the latter can expand the transmission range in the region of long waves.

Based on a general solution presented in terms of non-specified Green's functions, we consider the wave localization in some continuous elastic bodies and a regular lattice. We determine the localization-related frequency ranges and the localization degree in dependence on the frequency. While 2D-models are considered throughout the text, the axisymmetric localization phenomenon in the 3D-space is also mentioned.

The dynamic field created in such a structured system by an external harmonic force is obtained consisting of three different parts: the localized wave, a diverging wave, and non-spreading oscillations. Expressions for the wave amplitudes and the energy fluxes in the waves are presented.

1 Introduction

It has long been observed that a tsunami wave propagating above an underwater ridge is more intense (see Garipov, 1965, and Babich and Bilyi, 1979). Such a phenomenon is also observed and discussed with respect to seismic waves (Larose, et al., 2004, Adams et al., 2007, Fu et al., 2013), which appeared more intensive at a Earth surface elevation.

An example of the acoustic wave localization in water is the SOFAR channel (see, e.g., Munk, 1974, and Barros and Gendron, 2019), which is a horizontal layer in deep water where

the speed of sound attains its minimum; such a waveguide for sound may allow low frequency waves to propagate across a long distance.

The fact that the localization phenomenon manifests itself in various areas suggests that it has a universal nature. It occurs as far as there exists an inhomogeneity decreasing the wave phase speed. For the tsunami example, this effect follows from the fact that the smaller the depth, the lower the speed of surface waves, which, in turn, creates the waveguide.

An elastic body with an attached dynamic structure was possibly first considered in Slepyan (1967), where the evolution of a step wave propagating in an elastic bar with an oscillating medium has been examined (also see Slepyan, 1972). Today, this topic is under intensive development. Milton and Willis (2007) introduced a 3D elastic medium with discretely embedded mass-spring microstructure with not only linear but also angular degrees of freedom. Later we developed the classical wave equations of dynamic elasticity (Sobolev, 1937) for a medium with a uniformly distributed dynamic microstructure, Mishuris et al. (2019).

Evans and Porter (2007) considered waves in a flexural elastic plate rested on a discrete foundation and equipped by rigid point masses attached to it on a line. The work includes a comprehensive analysis of localized Floquet−Bloch waves within a one-dimensional grating in a flexural plate, as well as scattering of a plane wave at different angles of the incidence, which includes blockages and evaluation of transmission and reflection coefficients.

In the classical shallow water approximation, the equation (9) demonstrates non-dispersive behaviour of water waves. The recent paper, Porter (2019), has demonstrated the effect of variable morphology on wave scattering, with anisotropic effects, which are absent in the standard shallow-water equation. In the frequency domain, the extended shallow water equation coefficients incorporate the terms describing the depth variation. The paper, Porter (2019), has also proposed a connection of the wave scattering with the design of the water wave metamaterials.

Note that in one of the specific problems discussed in the present paper, we also consider an elastic plate. However, instead of the rigidly attached masses, we consider oscillators, which induce frequency-dependent inertia. In our case, the formulation used by Evans and Porter (2007) follows as the limit where the oscillator spring stiffness tends to infinity.

In the articles by Haslinger et al. (2015) and (2017), several settings for the point scatterers making up the semi-infinite periodic arrays were considered. In particular, the second one dealt with four classes of resonators arranged periodically in the flexural elastic plate: point masses embedded into the plate, multiple point mass-spring resonators attached to the top surface of the plate, point masses with a Winkler foundation (also see Biot, 1937) and multiple mass-spring resonators attached to both faces of the plate at the same point. It was also shown there that, for certain frequency regimes, some of the cases of resonators are equivalent to one another.

Although the work by Haslinger et al. (2015, 2017) did not deal with the wave localization, the kernel functions constructed in the Wiener-Hopf formulations include the relevant information about the Floquet−Bloch waves in the flexural system with resonators.

In the paper by Mishuris at al. (2019), it was shown, in particular, that in the sub-resonant regime, the wave phase speed reduction exists in the case of a class of dynamic microstructures, which leads to the localization.

In the current paper, we first discuss general conditions (valid for linear waves of any

nature) under which a 2D free sinusoidal wave exponentially localizes at the wave vector line. We also show that the conclusion also relates to the 3D case. Then we present a general formulation for a system comprised of two interconnected elastic structures. One, the *body*, is uniform and orthotropic in the (x_1, x_2)-plane. Another, the *structure*, is a set of dynamic inhomogeneities uniformly distributed along the x_1-line. Each component of the *system*, the body and the structure, can be continuous or discrete. For such a system, presented by (non-specified) Green's functions for its components, we study free sinusoidal waves propagating along the structure line (x_1 is also assumed to be a line of symmetry for the discrete body)[1].

This formulation allows us to derive the dispersive relation for the system (in terms of the partial Green functions) and to make some general conclusions about the role of the attached structure. Further, specifying the structure (but not the body) as the line-distributed oscillators, we come to conclusions concerning the localization in this partly-specified system and some of its limiting cases.

Based on the general results, we consider in detail problems involving a membrane, a discrete lattice, and a flexural plate. Finally, we study a forced wave in a line-structured membrane, where the forced dynamic field is considered. In certain frequency ranges, it consists of three parts: the localized wave, a divergent wave, and non-spreading oscillations.

2 General considerations

2.1 Evanescent waves in two dimensions

Here and below, in the case of a periodic body structure, Floquet−Bloch wave is assumed instead of the regular sinusoidal wave. Accordingly, the space points $\mathbf{x}$ belong to the corresponding discrete set of the reference points, and we expect the wavenumbers to be in the symmetrical period, $-\pi/a_{1,2} < k_{1,2} < \pi/a_{1,2}$, where $a_{1,2}$ are the corresponding periods of the body structure.

In reference to the dynamics of an elastic body (homogeneous or periodic in the x_1, x_2-plane), we assume that two conditions are valid. The first is space-time inversion symmetry: $t \Leftrightarrow -t$, $\boldsymbol{x} \Leftrightarrow -\boldsymbol{x}$, condition $(*)$. Under this condition, the dispersion dependence (or the considered branch of it) for the complex wave

$$\boldsymbol{u}(t, x_1, x_2) = \boldsymbol{A}\mathrm{e}^{i(\omega t - k_1 x_1 - k_2 x_2)} \tag{1}$$

can be expressed as

$$\omega^2 = \omega^2(k_1^2, k_2^2)\,. \tag{2}$$

The second is that in the considered branch of the dispersion relation, the square of the frequency is an increasing function of both real arguments; that is, the stiffness is as large as the wavelength is small, condition $(**)$.

[1]Such a general consideration represents another example, confirming that "Greater generality brings simplicity" (Slepyan, 2019). We can add that the generality brings not only simplicity but a better understanding of causes and consequences.

It follows from the latter that for a fixed frequency there is a single-valued dependence $k_2^2(k_1^2)$. In particular, for a real k_2, k_1^2 reaches maximum, $k_1^2 = k_{1m}^2$, at $k_2 = 0$, that is for a wave propagating in the $\pm x_1$-directions. Other cases, where k_1^2 is lower, correspond to $k_2^2 > 0$, that is to different wave vectors.

At the same time, under the fixed frequency, the dispersion relation is also valid for $k_1^2 > k_{1m}$ with $k_2^2 < 0$, which corresponds to a wave propagating in the x_1-direction, where the wave's amplitude depends exponentially on x_2.

2.1.1 3D space axisymmetric wave

The above conclusion also relates to a wave propagating in a 3D space. Indeed, consider for example the axisymmetric wave equation for the elasticity scalar wave potential ϕ

$$\frac{1}{r}\frac{\partial}{\partial r}\left(r\frac{\partial \phi}{\partial r}\right) - \left(k^2 - \frac{\omega^2}{c^2}\right)\phi = 0\,, \quad \phi = \phi(r)\mathrm{e}^{\mathrm{i}(\omega t - kx)}\,, \tag{3}$$

where r is the radial coordinate, k is the wavenumber and c is the wave speed. For the r-independent plane wave $\omega = ck$, and we denote $k = k_* = \omega/c$.

For $k^2 < k_*^2$ the above equation has a regular solution

$$\phi = J_0\left(r\sqrt{\frac{\omega^2}{c^2} - k^2}\right)\mathrm{e}^{\mathrm{i}(\omega t - kx)}\,. \tag{4}$$

Let a structure exist at the x-axis, such that elevates the wavenumber under the fixed frequency, $k^2 > k_*^2$. In this case, the wave is exponentially localized at the axis

$$\phi = K_0\left(r\sqrt{k^2 - \frac{\omega^2}{c^2}}\right)\mathrm{e}^{\mathrm{i}(\omega t - kx)}\,. \tag{5}$$

2.1.2 2D space Evanescent waves. Continuation

We now return to our problem of the body with a *structure* uniformly distributed (continuously or discretely) on the line $x_1 = 0$. For the complex wave (1) propagating along the structure line, the force Q and/or moment $\mathcal{M}$, through which the structure acts on the body, have similar dependence

$$Q[\mathcal{M}] = Q_0[\mathcal{M}_0](x_2)\mathrm{e}^{i(\omega t - k_1 x_1)}\,. \tag{6}$$

Accordingly, the wave, if it exists, is symmetric in x_2 for Q and antisymmetric for $\mathcal{M}$.

The main role belongs to the wave vector component, k_1, that corresponds to the structured body under a given frequency. If $0 < k_1^2 < k_{1m}^2$, the component k_2 is real: $k_2 = \pm\sqrt{k_{1m}^2 - k_1^2}$. In our case, this would correspond to waves propagating at angles to the x_1-axis with nonzero group velocities, as it follows from the condition (**). So, in this case, if it could exist, there would be energy flux from the structure to infinity or from infinity into the structure, which is not the case in the steady-state regime of the system under consideration. The equality $k_1^2 = k_{1m}^2$ is also unacceptable since it corresponds to the uniform body. The only inequality $k_1^2 > k_{1m}^2$ remains.

Thus, there exists a steady-state wave in a body equipped with an inhomogeneity uniformly distributed on a line, and it is exponentially localized at this line. The necessary and sufficient condition for such a wave to exist is that the wavelength is less than it would be in a free body (for the same frequency):

$$k_1^2 > k_{1*}^2 \,. \tag{7}$$

Under a fixed frequency, there is a one-to-one correspondence between the wavenumber and phase velocity. Namely, a decrease in the latter corresponds to an increase in the former. This correspondence allows us to rewrite the condition (7) in the equivalent form

$$c_p < c_{p*} \,, \tag{8}$$

where c_{p*} is the phase speed of the wave in the free body.

In solid mechanics, the localization can be obtained, in particular, with a structure composed of a line of added masses or a positive frequency-dependent masses corresponding to the sub-resonant regime of oscillators. Clearly, according to the condition (**), the increase in the mass under the frequency fixed must be compensated by a decrease in the wavelength.

In fluid mechanics, the dispersion relation for a gravity wave in finite-depth water is

$$\omega^2 = gk \tanh(hk) \,, \tag{9}$$

where g and h are the gravity acceleration and the depth, respectively. It follows that for a given ω the phase speed lowers as the depth decreases. Thus, for a water 'body' on an underwater ridge, inequality (8) is true, and the tsunami phenomenon mentioned in the introduction would occur as it does.

Note that in the classical shallow water approximation, the equation (9) demonstrates non-dispersive behaviour of water waves. The recent paper, Porter (2019), has demonstrated the effect of variable morphology on wave scattering, with anisotropic effects, which are absent in the standard shallow-water equation. In the frequency domain, the extended shallow water equation coefficients incorporate the terms describing the depth variation. Porter (2019) has also proposed a connection of the wave scattering with the design of the water wave metamaterials.

2.2 The governing equation

2.2.1 The Green functions

Let $G(t, x_1, x_2)$ and $G_0(t)$ be the Green functions for the body and the structure, respectively, where the latter corresponds to a unit pulse applied to the free structure at the structure-body contact point. Then the displacements expressed by the force Q (6) are as follows (the proceedings for moment $\mathcal{M}$ are similar)

$$u(t, x_1, x_2) = G(t, x_1, x_2) ** Q(t, x_1) \,, \quad u(t, x_1) = -G_0(t) * Q(t, x_1) \,, \tag{10}$$

where for the continuous body, the symbol $**$ denotes the convolution double integral on t and x_1. For a discrete body it involves a convolution integral over t and the corresponding sum over discrete coordinate x_1. The single asterisk $*$ indicates the convolution over t.

The Laplace transform on t and the Fourier transform on x_1 result in

$$u^{LF}(s,k_1,x_2) = G^{LF}(s,k_1,x_2)Q^{LF}(s,k_1)\,, \quad u^{LF}(s,k_1,0) = -G_0^L(s)Q^{LF}(s,k_1)\,. \tag{11}$$

2.2.2 The dispersion relation and wave localization

The dispersion relation for the system, the connection between ω and k_1, follows (with $s \to \mathrm{i}\omega$) from the fact that at $x_2 = 0$ the displacements of the body and the structure coincide. The relationship is

$$\boxed{G^{LF}(\mathrm{i}\omega,k_1,0) + G_0^L(\mathrm{i}\omega) = 0\,.} \tag{12}$$

Thus, the wave must obey the dispersion relation (12) for $x_2 = 0$, which defines the real wavenumber k_1, while the wavenumber k_2 must correspond to equations for the free body. It is crucial that, in a frequency region, the latter appears complex. Indeed, for a sub-resonant frequency, the structure is dynamically equivalent to a (positive) frequency-dependent mass; hence, the above equations define a real wavenumber $k_1^2 > k_{1*}^2$ (7) and $k_2^2 < 0$, which corresponds to the localized wave.

2.2.3 Continuous body with a discretely attached structure

In this case, the discrete Fourier transform can be expressed through the continuous version (see, e.g., Eq. 28 in Slepyan, 2018)

$$f^{Fd}(k) = \sum_{n=-\infty}^{\infty} f(an)\mathrm{e}^{\mathrm{i}kan} = \frac{1}{a}\sum_{n=-\infty}^{\infty} f^F\left(k + \frac{2\pi n}{a}\right) \tag{13}$$

The expression of the Green function is

$$G^{LF_d}(\mathrm{i}\omega,k_1,x_2) = \sum_{n=-\infty}^{\infty} G^L(\mathrm{i}\omega,an,x_2)\mathrm{e}^{\mathrm{i}k_1an} = \frac{1}{a}\sum_{n=-\infty}^{\infty} G^{LF}\left(\mathrm{i}\omega,k_1+\frac{2\pi n}{a},x_2\right)\,. \tag{14}$$

Note that the Green functions for the continuous and discrete microstructures have different dimensions.

2.3 Structure as a line of non-connected oscillators

In this section, we specify the structure as (discretely or continuously) line-distributed mass-spring oscillators, Fig. 1

The Green function for the oscillator G_0, that is the displacement of the end point of the oscillator spring (at which it is attached to the body) under the pulse $Q = \delta(t)$ is

$$G_0(t) = \frac{1}{\varkappa_0}\delta(t) + \frac{t}{m_0} \quad \Longrightarrow \quad G_0^L(s) = \frac{s^2+\omega_0^2}{\varkappa_0 s^2}\,, \quad \omega_0^2 = \frac{\varkappa_0}{m_0}. \tag{15}$$

Note that for a continuous system three partial formulations follow as the limiting cases: (1) The line of attached rigid masses (where spring stiffness $\varkappa_0 \to \infty$): $G_0^L(s) \to 1/(m_0 s^2)\,.$

(2) The line-localized Winkler foundation (where oscillator mass $m_0 \to \infty$: $G_0^L(s) \to 1/\varkappa_0$.
(3) The line of fixed points of the body (where both $\varkappa_0$ and m_0 tend to infinity): $G_0^L(s) \to 0$.

We see that the first case corresponds to rigidly attached masses, which elevates the wavenumber (reduces the phase speed), and results in wave localization. In the second case, the structure corresponds to the Winkler foundation, which cannot decrease the phase speed, and this conclusion is still valid when the foundation stiffness increases unboundedly (as in the last case).

Thus, localization can take place only in the first limiting case. However, in the sub-resonance regime, $\omega < \omega_0$, where the frequency-dependent added mass is positive, the localization occurs under finite parameters too.

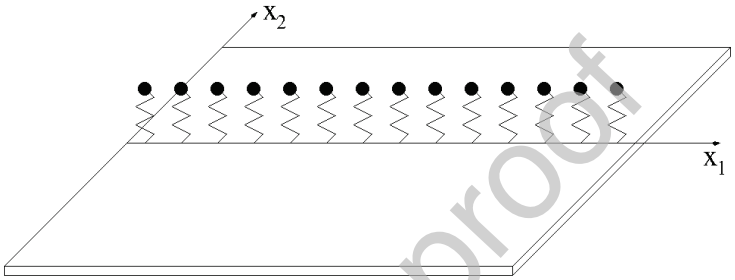

Figure 1: The body (shown here as a plate) with the uniformly distributed occillators.

Below along with the frequency ω, we use the dimensionless one and denote

$$G_0^L(\mathrm{i}\omega) = -\frac{1}{\varkappa_0 \mathcal{R}(\Omega)}\,, \tag{16}$$

where the notations

$$\mathcal{R}(\Omega) = \frac{\Omega^2}{1-\Omega^2}\,, \quad \Omega = \frac{\omega}{\omega_0}\,, \tag{17}$$

are used throughout the paper.

3 Some specified structured system

3.1 Membrane with continuous line of oscillators

The Green function $G(t, x_1, x_2)$ of the free membrane satisfies the equation

$$m\frac{\partial^2 G}{\partial t^2} - T_1\frac{\partial^2 G}{\partial x_1^2} - T_2\frac{\partial^2 G}{\partial x_2^2} = \delta(t)\delta(x_1)\delta(x_2)\,, \tag{18}$$

where m is the mass per unit area and $T_{1,2}$ are the (positive) tensile forces. It follows that

$$G^{LFF}(s, k_1, k_2) = \frac{1}{ms^2 + T_1 k_1^2 + T_2 k_2^2}, \tag{19}$$

and for $x_2 = 0$

$$G^{LF}(s, k_1, 0) = \frac{1}{\pi}\int_0^\infty G^{LFF}(s, k_1, k_2)\,\mathrm{d}k_2 = \frac{1}{2\sqrt{T_2(ms^2 + T_1k_1^2)}}\,. \tag{20}$$

The dispersion relation (12) becomes ($s \to \mathrm{i}\omega$)

$$\frac{1}{2\sqrt{T_2(T_1k_1^2 - m\omega^2)}} + \frac{\omega^2 - \omega_0^2}{\varkappa_0\omega^2} = 0\,. \tag{21}$$

This demonstrates that there is no sinusoidal wave in the super resonant regime, $\omega^2 > \omega_0^2$.

In dimensionless variables, the dispersion relation takes the form

$$\sqrt{K_1^2 - \Omega^2} = \gamma\mathcal{R}(\Omega)\,, \quad \gamma = \frac{\varkappa_0}{2\sqrt{T_2m\omega_0^2}} = \frac{1}{2}\sqrt{\frac{m_0\varkappa_0}{mT_2}}\,. \tag{22}$$

Here and below we define the dimensionless values as

$$K_{1,2} = k_{1,2}\sqrt{\frac{m_0T_1}{m\varkappa_0}}\,, \quad X_{1,2} = x_{1,2}\sqrt{\frac{m\varkappa_0}{m_0T_1}}\,. \quad \mathcal{T} = t\omega_0\,, \tag{23}$$

with the exponent in the wave expression (1)

$$\exp[\mathrm{i}(\omega t - k_1x_1 - k_2x_2)] = \exp[\mathrm{i}(\Omega\mathcal{T} - K_1X_1 - K_2X_2)]\,. \tag{24}$$

The dispersion diagram $\Omega = \Omega(K_1)$ is presented on Fig. 2.The ratio of the wave phase speed to that in the free membrane

$$\frac{c_p}{c_0} = \sqrt{1 + \gamma^2\mathcal{R}^2(\Omega)}, \quad c_0 = \sqrt{\frac{T_1}{m}}\,, \tag{25}$$

is plotted in Fig. 3 (left). We can see that the structure reduces the phase speed in the subcritical regime.

The dispersion relation for the free membrane, valid for $x_2 \neq 0$, is

$$m\omega^2 = T_1k_1^2 + T_2k_2^2\,. \tag{26}$$

Now, with reference to the expression in (21), for waves not growing with distance from the oscillator line, we find that in the sub-resonant regime, $\omega^2 < \omega_0^2$, the wave does exist with $m\omega^2 < T_1k_1^2$ and that it is exponentially localized. Namely, in the expression of the wave (1)

$$k_2 = \mp\frac{\mathrm{i}\varkappa_0}{2T_2}\mathcal{R}(\Omega) \quad (\pm\, x_2 > 0)\,. \tag{27}$$

The normalised (dimensionless) wave localization number

$$\alpha = |K_2| = \sqrt{\frac{T_1}{T_2}}\gamma\mathcal{R}(\Omega)\,, \quad (0 \le \Omega^2 < 1) \tag{28}$$

is also plotted in Fig. 3 (right). In these terms, the exponent (24) becomes $\exp[\mathrm{i}(\Omega\mathcal{T} - K_1X_1) - \alpha|X_2|]$.

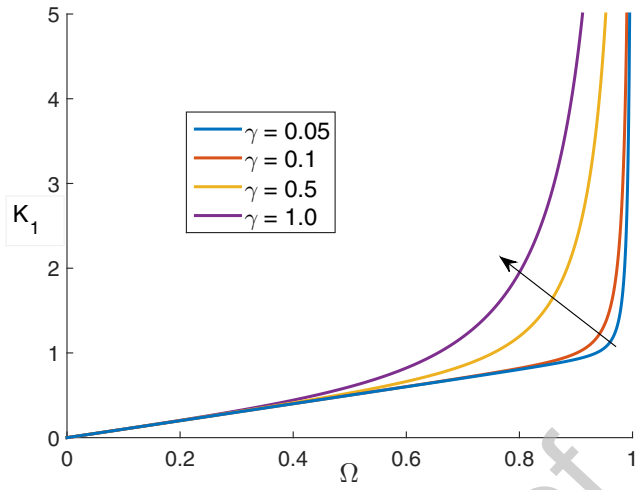

Figure 2: Dispersion diagram following from the equation (22). The curves with greater $K_1(\Omega)$ correspond to higher γ is shown by the arrow.

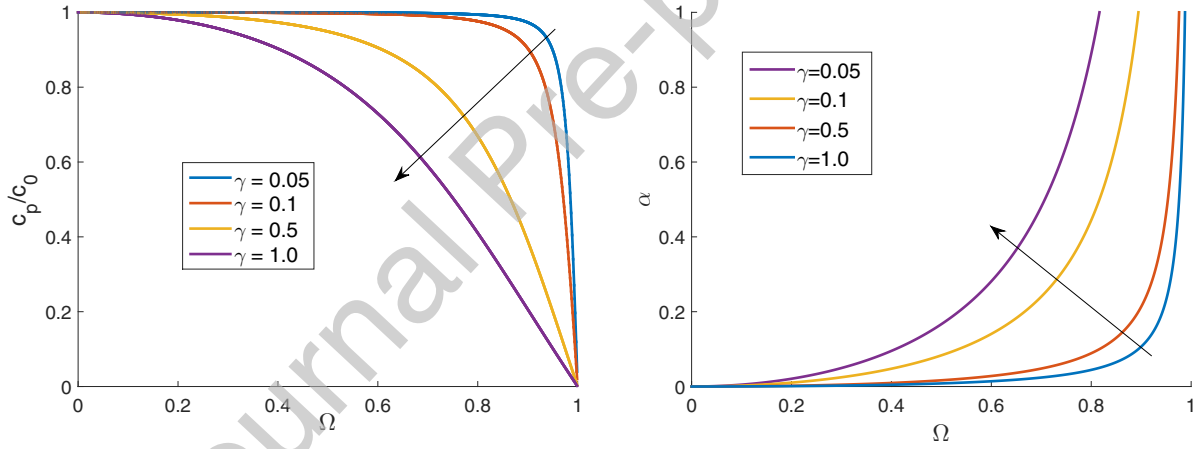

Figure 3: The ratio of the wave phase speed in the structured and free membranes (left), and the localization number α (right) as functions of the normalised frequency. Parameter γ grows as shown by the arrow. The plots correspond to $T_1 = T_2$.

3.2 Square-cell lattice

Consider a uniform square-cell lattice, the normal displacement of which obeys the dynamic equation

$$M\frac{\mathrm{d}^2 u_{m,n}}{\mathrm{d}t^2} = \varkappa(u_{m+1,n} + u_{m-1,n} + u_{m,n+1} + u_{m,n-1} - 4u_{m,n})\,, \quad m,n = 0,\pm1,\pm2,\dots\,, \quad (29)$$

where M is the mass and $\varkappa$ is the stiffness of the inter-mass links. In the following, the cell size is denoted by a. The transformed lattice Green function is

$$G^{LF_dF_d}(s,k_1,k_2)=\frac{1}{Ms^2+4\varkappa\sin^2(ak_1/2)+4\varkappa\sin^2(ak_2/2)}, \tag{30}$$

with the dispersion relation for the free lattice

$$\omega=\pm\omega_L\sqrt{\left(\sin^2(ak_1/2)+\sin^2(ak_2/2)\right)}\,,\quad \omega_L=\sqrt{\frac{4\varkappa}{M}}\,, \tag{31}$$

where ω_L is the limiting frequency of the lattice at $k_1=\pi/a, k_2=0$ (or vice versa).

Further

$$G^{LF_d}(s,k_1,0)=\frac{a}{\pi}\int_0^{\pi/a}G^{LF_dF_d}(s,k_1,k_2)\,\mathrm{d}k_2=$$
$$\frac{1}{4\varkappa}\left[\left(-\frac{\Omega^2}{\Omega_L^2}+\sin^2(ak_1/2)\right)\left(1-\frac{\Omega^2}{\Omega_L^2}+\sin^2(ak_1/2)\right)\right]^{-1/2},\quad \Omega_L=\frac{\omega_L}{\omega_0}\,. \tag{32}$$

Now, with reference to (12), (32) and (16), we reach the dispersion relation for the lattice-oscillator system

$$4\varkappa\left[\left(-\frac{\Omega^2}{\Omega_L^2}+\sin^2(ak_1/2)\right)\left(1-\frac{\Omega^2}{\Omega_L^2}+\sin^2(ak_1/2)\right)\right]^{1/2}-\varkappa_0\mathcal{R}(\Omega)=0\,. \tag{33}$$

We find

$$\sin^2(K_1/2)=\frac{\Omega^2}{\Omega_L^2}+\frac{1}{2}\left(\sqrt{1+\left(\frac{\mathcal{R}(\Omega)}{\lambda}\right)^2}-1\right),\quad \lambda=\frac{\varkappa}{\varkappa_0},\quad K_1=ak_1\,. \tag{34}$$

In this relation, K_1 is real if the sinusoidal wave exists. From this and (33) the inequalities follow which define the range of the frequency

$$\Omega^2<\min\left(1,\Omega_L^2\right)\quad\text{and}\quad\left(\frac{\mathcal{R}(\Omega)}{\lambda}\right)^2\le\left(1+2\left(1-\frac{\Omega^2}{\Omega_L^2}\right)\right)^2-1\,. \tag{35}$$

The frequency upper bound, Ω_{max}, plotted in the $(\Omega_L,\,\lambda)$ plane is presented in Fig. 4.

The following asymptotic representations are valid

$$\Omega_{max}^2-\frac{\sqrt{8}\,\lambda}{1+\sqrt{8}\lambda}\sim-\frac{6\lambda^2}{\Omega_L^2(1+\sqrt{8}\,\lambda)^3}\,,\quad \Omega_L\to\infty\,,\quad \lambda<\infty$$
$$\Omega_{max}^2-1\sim-\frac{1}{\lambda}\left(\left(3-\frac{2}{\Omega_L^2}\right)^2-1\right)^{-1/2},\quad \lambda\to\infty\,,\quad \Omega_L>1,$$
$$\Omega_{max}^2-\Omega_L^2\sim-\frac{\Omega_L^5}{4\lambda^2\left(1-\Omega_L^2\right)^2}\,,\quad \lambda\to\infty\,,\quad 0<\Omega_L<1\,,$$
$$\Omega_{max}^2-1\sim-\frac{1}{\sqrt{8}\lambda}\left(1+\frac{3}{4\Omega_L^2}\right),\quad \Omega_L\to\infty,\quad \lambda\to\infty\,,$$
$$\Omega_{max}^2\sim\frac{4\Omega_L^2\lambda}{3\lambda+\sqrt{\lambda^2+2\,\Omega_L^4}},\quad \Omega_L\to 0,\quad \lambda\to 0\,. \tag{36}$$

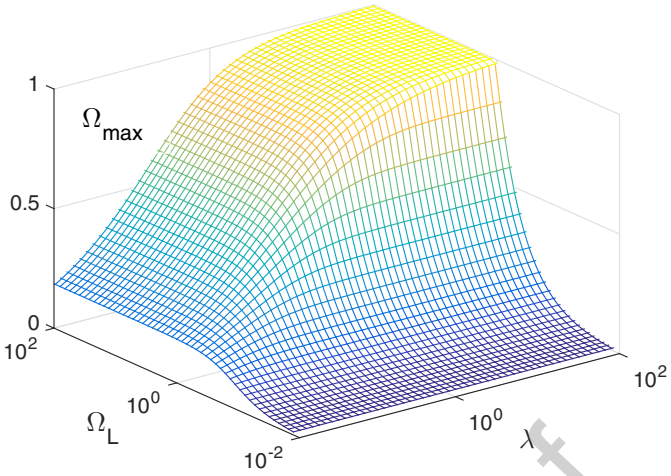

Figure 4: The upper bound of the domain $\Omega \in (0, \Omega_{max})$ where localized waves is presented as a function of the normalised material parameters Ω_L and α.

The dispersion curves, $K_1(\Omega)$, are shown in Fig. 5, where $0 < K_1 < \pi$, while the range of the frequency Ω is defined in (35).

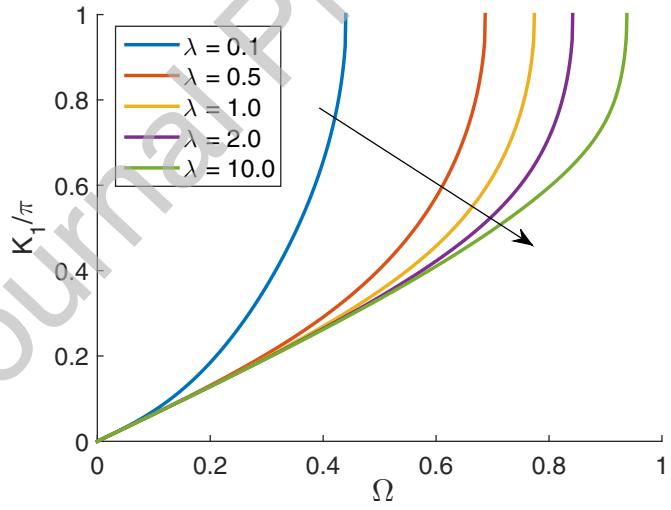

Figure 5: The dispersion diagram for the structured lattice plotted for $\Omega_L = 1$ and several values of λ. The latter grows in the direction shown by the arrow.

3.2.1 Phase velocities and the localization number

With reference to (31) and (34), the ratio of the wave phase speed to that in the free lattice is

$$\frac{c_p}{c_{p0}} = \arcsin\left(\frac{\Omega}{\Omega_L}\right)\left(\arcsin\sqrt{\frac{\Omega^2}{\Omega_L^2}+\frac{1}{2}\left(\sqrt{1+\left(\frac{\mathcal{R}(\Omega)}{\lambda}\right)^2}-1\right)}\right)^{-1}. \tag{37}$$

The wave phase speed ratio, that of the phase speed in the structured lattice to that in the free lattice (under the same frequency), is shown in Fig. 6. It can be seen that the structure reduces the phase speed as would be expected.

Taking into account the dispersion relation for the free lattice (31) and the expression for K_1 (34), we now find that there exists a localized wave with the imaginary wavenumber K_2, where

$$\sin(K_2/2) = \mp \mathrm{i}\left(\frac{1}{2}\left(\sqrt{1+\left(\frac{\mathcal{R}(\Omega)}{\lambda}\right)^2}-1\right)\right)^{1/2} \quad (\pm x_2 > 0)\,. \tag{38}$$

The dimensionless localization number, $\alpha = |K_2|$, and the Floquet - Bloch wave are

$$\cosh(\alpha) = \sqrt{1+\left(\frac{\mathcal{R}(\Omega)}{\lambda}\right)^2}, \quad u = U_0 \mathrm{e}^{\mathrm{i}(\omega t - K_1 X_1) - \alpha|X_2|}\,, \quad U_0 = \mathrm{const}\,. \tag{39}$$

The dependence $\alpha(\Omega)$ for $\lambda = 1$ is plotted in Fig. 6, right (λ is defined in (34)). In accordance with the general conclusion, the localization is caused by the phase speed decrease. It is as strong as the parameter λ is low.

3.3 Elastic flexural plate

The scattering of flexural waves by an infinite row of point masses, rigid pins or a row of springs connecting a plate to a rigid foundation, was studied in detail by Evans and Porter (2007). Also, the study of scattering of flexural waves by semi-infinite arrays of multiple spring-mass resonators connected to the master plate was included in the paper by Haslinger et al. (2017). The latter focused on transmission-reflection at a structured interface, which was orthogonal to individual semi-infinite gratings in the flexural plate. We here consider the wave localization in a plate equipped by the line of oscillators.

From the plate equation

$$m\frac{\partial^2 u}{\partial t^2} + D\left(\frac{\partial^4 u}{\partial x_1^4} + 2\frac{\partial^4 u}{\partial x_1^2 \partial x_2^2} + \frac{\partial^4 u}{\partial x_2^4}\right) = q\,, \tag{40}$$

where m and q are the mass and load per unit area, respectively, and D is the bending stiffness, in the same way as above, we obtain that for $m\omega^2 < Dk_1^4$

$$G^{LF}(\mathrm{i}\omega, k_1, 0) = \frac{\sqrt{k_1^2+\beta\omega}-\sqrt{k_1^2-\beta\omega}}{4\omega\sqrt{Dm}\sqrt{k_1^4-\beta^2\omega^2}}, \quad \beta = \sqrt{\frac{m}{D}}\,, \tag{41}$$

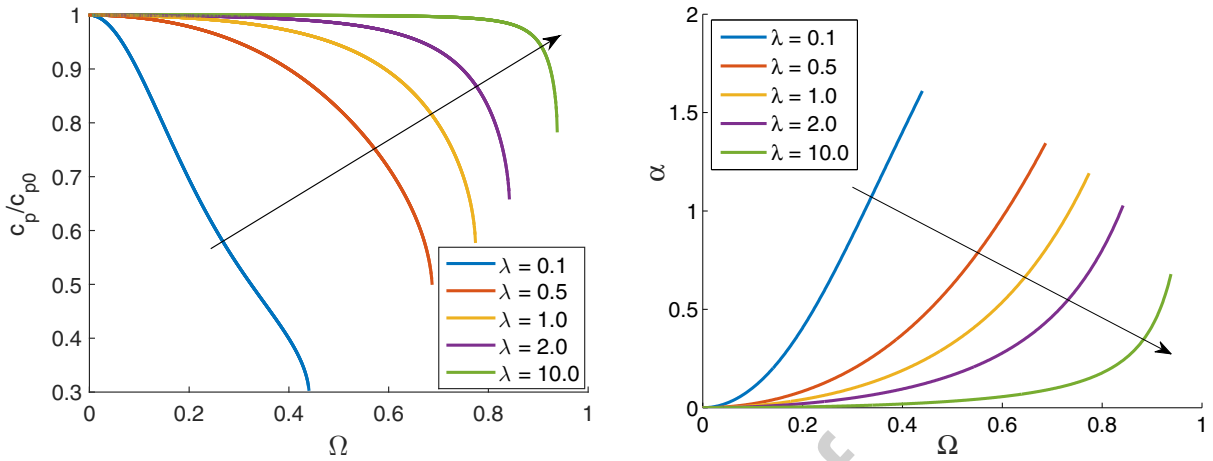

Figure 6: The ratio of the phase speeds of the structure to that in the free lattice (left) and the localization number α (right) as functions of the normalised frequency. Parameter λ grows as shown by the arrow.

or, in dimensionless variables,

$$G^{LF}(\mathrm{i}\omega, k_1, 0) = \frac{\sqrt{K_1^2+\Omega}-\sqrt{K_1^2-\Omega}}{4D(\beta\omega_0)^{3/2}\sqrt{K_1^4-\Omega^2}}, \qquad K_{1,2} = \frac{k_{1,2}}{\sqrt{\beta\omega_0}}\,. \tag{42}$$

The plate-oscillator system dispersion relation follows as

$$\frac{\sqrt{K_1^2+\Omega}-\sqrt{K_1^2-\Omega}}{\sqrt{K_1^4-\Omega^2}} - \frac{\eta}{\mathcal{R}(\Omega)} = 0\,, \quad \eta = \frac{4D(\beta\omega_0)^{3/2}}{\varkappa_0} = 4\left(\frac{Dm^3}{\varkappa_0 m_0^3}\right)^{1/4}, \tag{43}$$

while the dispersion relation for the free plate is

$$\Omega^2 = (K_1^2+K_2^2)^2\,. \tag{44}$$

3.3.1 Phase velocities and the localization number

Note that as $\Omega \to 0$, the dispersion relation (43) approaches that of the free plate

$$K_1 = \sqrt{\Omega} + \frac{1}{\eta^2}\,\Omega^2 + O\left(\Omega^{11/4}\right), \quad (\Omega \to 0), \tag{45}$$

and therefore

$$\frac{c_p}{c_{p0}} = 1 - \frac{1}{\eta^2}\,\Omega^{3/2} + O\left(\Omega^{9/4}\right), \quad (\Omega \to 0)\,, \quad c_{p0} = \sqrt{\frac{\omega}{\beta}}\,, \tag{46}$$

where the phase speed c_{p0} corresponds to the free plate. The (exact) ratio of the wave phase speed to that of the free plate, c_p/c_{p0}, is plotted in Fig. 8.

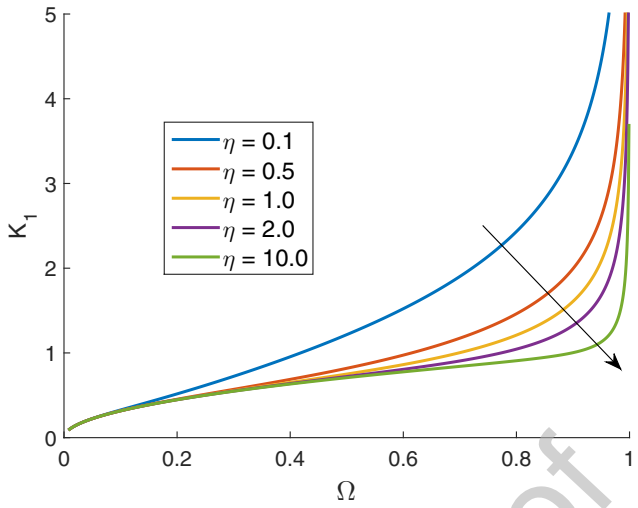

Figure 7: The dispersion diagram for the structured plate for several values of parameter η (the direction of its growth is shown by the arrow).

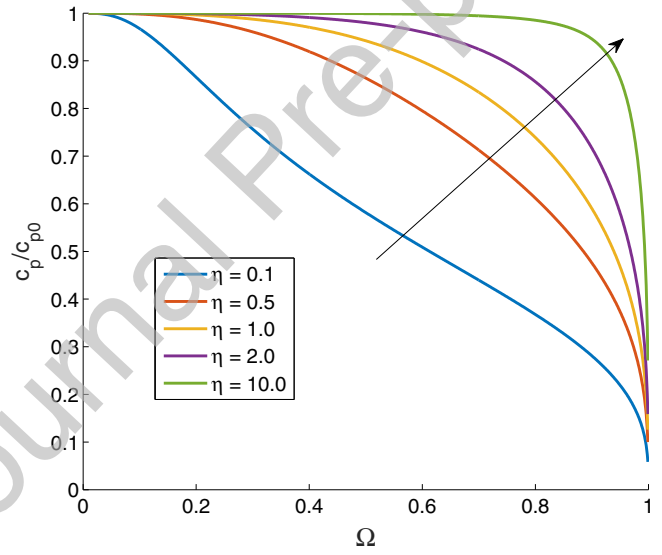

Figure 8: The ratio of the phase speeds in the structural plate to that in the free one as functions of the normalised frequency. The parameter η grows as shown by the arrow.

The wave localization is defined by the two couples of the imaginary wavenumbers

$$k_{21} = \pm \mathrm{i}\alpha_1, \quad \alpha_1 = \sqrt{k_1^2 - \beta\omega}\,, \quad k_{22} = \pm \mathrm{i}\alpha_2, \quad \alpha_2 = \sqrt{k_1^2 + \beta\omega}\,. \tag{47}$$

In sum, the corresponding waves must satisfy the condition $\partial u/\partial x_2 = 0$ ($x_2 = 0$). Thus, the localized wave displacement is

$$u = \frac{A}{\alpha_2 - \alpha_1}\left(\alpha_2 \mathrm{e}^{-\alpha_1|x_2|} - \alpha_1 \mathrm{e}^{-\alpha_2|x_2|}\right), \tag{48}$$

where A is the wave amplitude. Note that as follows from this expression $\partial u/\partial x_2 = 0$ at $x_2 = \pm 0$ as it should be.

In Fig. 9, based on the normalisation in (42), we present the localization numbers, α_1 (left) and α_2 (right) for some values of the parameter η, (43).

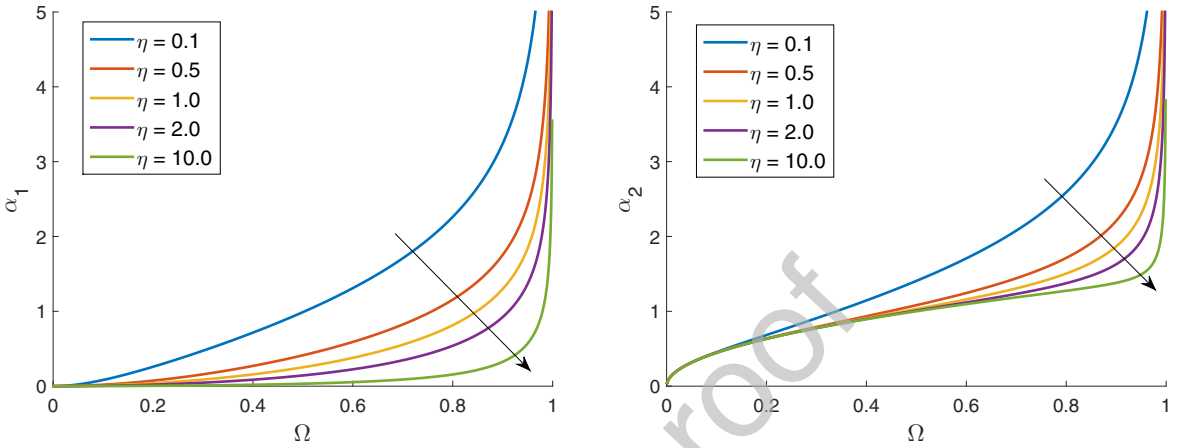

Figure 9: The normalised localization numbers α_1 and α_2 as functions of the normalised frequency. The parameter η grows as shown by the arrow.

4 Forced wave

4.1 Formulation and solution

Consider a rested on the Winkler foundation membrane structured by the oscillators uniformly distributed on the line $x_2 = 0$. Let an external force, $P\mathrm{e}^{\mathrm{i}\omega t}$, act on the membrane at the origin, $x_1 = x_2 = 0$.

Note that the below solution, regular outside the loaded point, has at the origin a weak singularity of the displacement, u, which is infinite at this point. Nevertheless, as can be seen below, the rate of energy produced by the point force, $N = \Re P\mathrm{e}^{\mathrm{i}\omega t}\,\overline{\partial u/\partial t}$, is finite.

With reference to (18) and (15), we write the dynamic equation in the form

$$m\frac{\partial^2 u}{\partial t^2} - T_1\frac{\partial^2 u}{\partial x_1^2} - T_2\frac{\partial^2 u}{\partial x_2^2} + \varkappa u = -(\mathcal{R}_0(t) * u)\delta(x_2) + P\mathrm{e}^{\mathrm{i}\omega t}\delta(x_1)\delta(x_2), \tag{49}$$

where $u = u(t, x_1, x_2)$, $\mathcal{R}_0(t)$ corresponds to the oscillator's response, $\varkappa$ is the foundation stiffness, and $*$ is the convolution symbol (now the convolution on t).

The elastic foundation brings another natural frequency, $\omega = \omega_m = \sqrt{\varkappa/m}$, which corresponds to oscillations of the non-deformed membrane on the foundation. Note that the range $0 \le \omega < \omega_m$ represents a band gap, where no free sinusoidal waves can exist. So, the most interest range for us is $\omega_m < \omega < \omega_0$ (with $\omega_0 > \omega_m$).

Due to the symmetry of the system relative to the axes, the dynamic field is also symmetric. This fact allows us to consider only the first quadrant of the $x_{1,2}$-plane. Without loss of generality, we also assume that $\omega > 0$.

In terms of the integral transforms, the Laplace transform on t and Fourier transforms on x_1 and x_2, the equation becomes

$$(ms^2 + T_1k_1^2 + T_2k_2^2 + \varkappa)u^{LFF}(s,k_1,k_2) = -\mathcal{R}_0^L(s)u^{LF}(s,k_1,0) + \frac{P}{s-\mathrm{i}\omega}\,,$$

$$\mathcal{R}_0^L(s) = \frac{1}{G_0^L(s)} = \frac{\varkappa_0 s^2}{\omega_0^2 + s^2}\,, \tag{50}$$

where $\Re s > 0$ and the expression $u^{LF}(s,k_1,0)$ means $u^{LF}(s,k_1)$ at $x_2 = 0$.

The Fourier inverse transform on k_2 for $x_2 = 0$ results in

$$u^{LF}(s,k_1,0) = \frac{1}{2\pi}\int_{-\infty}^{\infty} u^{LFF}(s,k_1,k_2)\,\mathrm{d}k_2$$

$$= \frac{1}{2T_2\alpha}\left(-\mathcal{R}_0^L(s)u^{LF}(s,k_1,0) + \frac{P}{s-\mathrm{i}\omega}\right)\,,\quad \alpha(k_1) = \sqrt{\frac{ms^2 + T_1k_1^2 + \varkappa}{T_2}}\,. \tag{51}$$

Taking into account that for $x_2 > 0$ the equation (49) is homogeneous we find

$$u^{LF}(s,k_1,x_2) = \frac{P}{s-\mathrm{i}\omega}\,\frac{\mathrm{e}^{-\alpha x_2}}{2T_2\alpha(k_1) + \mathcal{R}_0^L(s)}\,. \tag{52}$$

The established regime corresponds to the residue at $s = \mathrm{i}\omega$. In this connection, we note that if $s = \mathrm{i}\omega$, where we take $\omega > 0$, the equations admit homogeneous solutions. To exclude them and to preserve the waves excited by the prescribed force under zero initial conditions, we take the solution, which obeys a causality principle (the Mandelshtam principle, Mandelshtam (1972)). Formally, when needed, we use the prelimiting solution as follows:

$$s = s' + \mathrm{i}\omega\,,\quad 0 < s' \to 0\,. \tag{53}$$

Note that the causality principle for a steady-state solution is discussed in Slepyan (2002), Sec. 3.3.2.

At the steady-state regime the expression for the displacement (52) becomes

$$u^F(t,k_1,x_2) = U^F(k_1,x_2)\mathrm{e}^{\mathrm{i}\omega t}\,,$$

$$U^F(k_1,x_2) = \frac{P}{2\phi\sqrt{T_1T_2}}\,\frac{\exp(-\alpha X_2)}{\alpha_0 - \psi\mathcal{R}(\Omega)}\,, \tag{54}$$

where

$$\alpha_0 = \alpha_0(K_1) = \sqrt{-\Omega^2 + \Omega_m^2 + K_1^2}\quad (\Omega^2 - \Omega_m^2 < K_1^2)\,,$$

$$\alpha = \alpha(K_1) = \sqrt{\frac{T_1}{T_2}}\alpha_0\,,\quad \Omega = \frac{\omega}{\omega_0}\,,\quad \Omega_m = \frac{\omega_m}{\omega_0}\,,\quad \omega_0 = \sqrt{\frac{\varkappa_0}{m_0}}\,,\quad \omega_m = \sqrt{\frac{\varkappa}{m}}\,,$$

$$\phi = \sqrt{\frac{m\varkappa_0}{m_0T_1}}\,,\quad \psi = \sqrt{\frac{m_0\varkappa_0}{4mT_2}}\,,\quad K_{1,2} = \frac{k_{1,2}}{\phi},\quad X_{1,2} = \phi x_{1,2}\,. \tag{55}$$

In accordance with the condition (53), on the real k_1-axis,

$$\alpha_0 = \mathrm{i}\beta_0\,, \quad \beta_0 = \sqrt{\Omega^2 - \Omega_m^2 - K_1^2} \quad (\Omega^2 - \Omega_m^2 > K_1^2)\,,$$
$$\alpha = \mathrm{i}\beta\,, \quad \beta = \sqrt{\frac{T_1}{T_2}}\beta_0\,, \tag{56}$$

with the analytical continuation on the integration path deformed as shown in Fig. 10.

There are four singular points on the k_1 complex plane: two branch points

$$k_1 = \pm k_* \mp \mathrm{i}0\,, \quad k_* = \phi K_*\,, \quad K_* = \sqrt{\Omega^2 - \Omega_m^2} \ \ (\Omega_m < \Omega)\,,$$
$$K_* = \mp\mathrm{i}\sqrt{\Omega_m^2 - \Omega^2} \ \ (\Omega < \Omega_m)\,, \tag{57}$$

and two poles

$$k_1 = \pm k_{**} \mp \mathrm{i}0\,, \quad k_{**} = \phi K_{**}\,, \quad K_{**} = \sqrt{\Omega^2 - \Omega_m^2 + \left(\psi\mathcal{R}(\Omega)\right)^2} \quad (\Omega > \Omega_{min})\,, \tag{58}$$

where the minimal frequency $\Omega = \Omega_{min} < \Omega_m$ corresponds to $K_{**} = 0$. Recall that the frequencies are assumed to be positive.

Note that the pole and branch point located at $K_1 = -K_{**} + \mathrm{i}0$ and $\Re K_1 = -K_*$, respectively, contribute to $x_1 < 0$, while $K_1 = K_{**} - \mathrm{i}0$ and $\Re K_1 = K_*$ contribute to $x_1 > 0$, see Fig. 10. So, for $\omega > \omega_m$ we make branch cuts from the branch points:

$$-K_* < K_1 < 0\,, \quad 0 < -\mathrm{i}K_1 < \infty \quad (\text{for} \ \ x_1 < 0)\,,$$
$$0 < K_1 < K_*\,, \quad 0 < \mathrm{i}K_1 < \infty \quad (\text{for} \ \ x_1 > 0)\,, \tag{59}$$

and deform the Fourier inverse transform path accordingly (the only parts of the latter are shown in Fig. 10, which contribute to the solution).

For $\omega \le \omega_m$ the branch points are pure imaginary and the integration path is paved at the left and right of the cut, such that

$$\Re K_1 = -0, \ \sqrt{\Omega_m^2 - \Omega^2} \le \Im K_1 < \infty \ \text{ and } \ \Re K_1 = +0, \ -\infty < \Im K_1 \le -\sqrt{\Omega_m^2 - \Omega^2}\,. \tag{60}$$

4.1.1 Displacement decomposition

Accordingly to the integration path shown in Fig. 10, we represent the membrane displacement, (52), as

$$U(x_1, x_2) = U_1(x_1, x_2) + U_2(x_1, x_2) + U_3(x_1, x_2)\,, \tag{61}$$

where $U_1(x_1, x_2)$ is defined by the residual at point $K_1 = K_{**}$. $U_2(x_1, x_2)$ corresponds to the integration over the real part of the right branch cut (see Fig. 10, right), $0 < K_1 < K_*$, and $U_3(x_1, x_2)$ is defined by the integration over the imaginary part of it, $K = \mathrm{i}\xi$, $\xi_{min} < \xi < \infty$ (ξ_{min} corresponds to the minimum of $\mathrm{i}K_1$, see (59) and (60)).

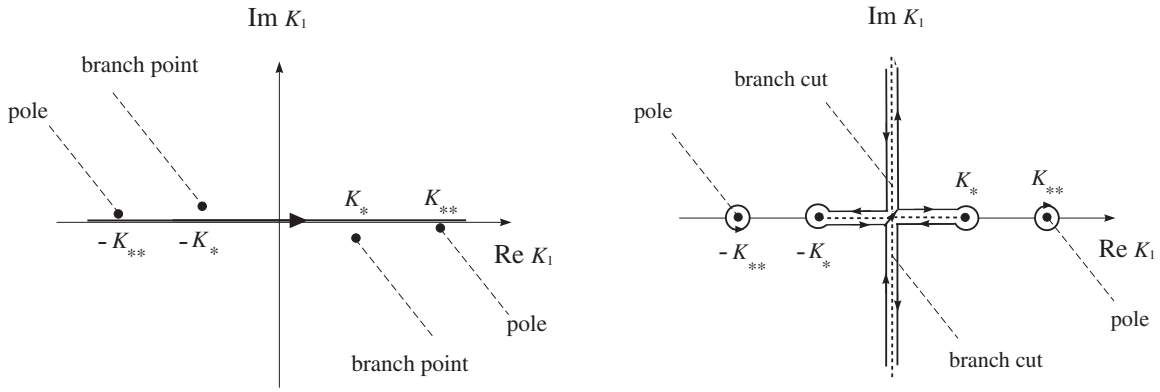

Figure 10: The pre-limiting locations of the poles and branch points and cuts (left). The contributed parts of the integration path (right). The negative (positive) singular points contribute to $x_1 < 0$ ($x_1 > 0$).

The displacements corresponding to these parts are as follows. The localized wave

$$U_1(x_1, x_2) = -\frac{\mathrm{i}P}{2\sqrt{T_1 T_2}} \frac{\psi\Omega^2}{1-\Omega^2} \frac{\exp(-\mathrm{i}K_{**}X_1 - \alpha(K_{**})X_2)}{K_{**}}\,, \tag{62}$$

where α, K_{**}, ψ and $X_{1,2}$ are defined in (55) and (58) .

The divergent wave

$$U_2(x_1, x_2) = -\frac{\mathrm{i}P}{2\pi\sqrt{T_1 T_2}} \int_0^{K_*} \Phi(K_1) \exp(-\mathrm{i}K_1 X_1)\, \mathrm{d}K_1 \quad (\Omega > \Omega_m)\,,$$

$$\Phi(K_1) = \frac{\beta_0(K_1)\cos(\beta(K_1)X_2) + \psi\mathcal{R}(\Omega)\sin(\beta(K_1)X_2)}{\beta_0^2(K_1) + \psi^2\mathcal{R}^2(\Omega)}\,, \quad U_2(x_1, x_2) = 0 \quad (\Omega \le \Omega_m)\,, \tag{63}$$

where (imaginary) $\beta_0(K_1)$ and $\beta(K_1)$ are defined in (56), and K_* for $\Omega > \Omega_m$ is presented in (57).

The non-spreading oscillations

$$U_3(x_1, x_2) = \frac{P}{2\pi\sqrt{T_1 T_2}} \int_\zeta^\infty \Phi(\mathrm{i}\xi) \exp(-\xi X_1)\, \mathrm{d}\xi\,,$$

$$\zeta = 0 \quad (\Omega_m \le \Omega)\,, \quad \zeta = \sqrt{\Omega_m^2 - \Omega^2} \quad (\Omega \le \Omega_m)\,. \tag{64}$$

On Fig. 11, we present the localized wave, $U_1(X_1, X_2)$, and the sum of the divergent wave and the oscillations, $U_+ = U_2(X_1, X_2) + U_3(X_1, X_2)$, for three different frequencies, $\Omega = 0.5, 0.7, 0.9$. The wave profiles at $x_2 = 0$ (left) and $x_1 = 0$ (right) are shown.

Note that in the membrane without the attached structure, a divergent wave and oscillations also exist, but the localized wave is absent.

4.2 Energy fluxes

4.2.1 General dependencies

We base on the following expressions of the energy fluxes (in this connection, see, e.g., Slepyan (2002), Sect. 3.1.5). The energy flux produced by the harmonic external force, $P\mathrm{e}^{\mathrm{i}\omega t}$, applied at $x_1 = x_2 = 0$ is

$$N_{in} = P\Re\left[\mathrm{e}^{\mathrm{i}\omega t}\overline{\dot{u}(t,0,0)}\right] = -P\omega\Im\overline{U(0,0)}\,, \quad u(t,0,0) = U(0,0)\mathrm{e}^{\mathrm{i}\omega t}\,. \tag{65}$$

Thus, only those parts of the displacement contribute to the waves, which correspond to the condition:

$$\Im U(0,0) < 0\,. \tag{66}$$

With account of the symmetry, the energy flux in waves propagating in x_1 and x_2 directions are, respectively,

$$\begin{aligned} N_{1out} &= -4\int_0^\infty \Re\left(\frac{\partial u(t,x_1,x_2)}{\partial t}T_1\overline{\frac{\partial u(t,x_1,x_2)}{\partial x_1}}\right)\mathrm{d}x_2 \\ &= 4\omega T_1\int_0^\infty \Im\left(U(x_1,x_2)\overline{\frac{\partial U(x_1,x_2)}{\partial x_1}}\right)\mathrm{d}x_2\,, \end{aligned} \tag{67}$$

and

$$\begin{aligned} N_{2out} &= -4\int_0^\infty \Re\left(\frac{\partial u(t,x_1,x_2)}{\partial t}T_2\overline{\frac{\partial u(t,x_1,x_2)}{\partial x_2}}\right)\mathrm{d}x_1 \\ &= 4\omega T_2\int_0^\infty \Im\left(U(x_1,x_2)\overline{\frac{\partial U(x_1,x_2)}{\partial x_2}}\right)\mathrm{d}x_1\,. \end{aligned} \tag{68}$$

4.2.2 Energy fluxes in the forced wave

First, we note that, as it follows from (64) and the above relations, part u_3, which contains the displacement singularity, does not contribute to the energy fluxes. This part represents oscillations, not a wave.

The wave u_1 and u_2 are orthogonal in energy. Namely, it appears that the work of the force on the localized wave $u_1(t,0,0)$ is equal to the energy flux in this wave

$$N_{1out} = N_{1in} = \frac{P^2\omega\varkappa_0}{4T_1T_2K_{**}\phi}\mathcal{R}(\Omega)\,, \quad K_{**} = \sqrt{\Omega^2 - \Omega_m^2 + \psi^2\mathcal{R}^2(\Omega)}\,. \tag{69}$$

It follows from this that the same conclusion is valid for the divergent wave u_2 (63)

$$\begin{aligned} N_{2out} = N_{2in} &= \frac{P^2\omega}{2\pi\sqrt{T_1T_2}}\int_0^{K_*}\frac{\beta_0(K_1)}{\beta_0^2(K_1) + \psi^2\mathcal{R}^2(\Omega)}\,\mathrm{d}K_1 \\ &= \frac{P^2\omega}{4\sqrt{T_1T_2}K_{**}}(K_{**} - \psi\mathcal{R}(\Omega)) \quad (\Omega \geq \Omega_m)\,, \end{aligned} \tag{70}$$

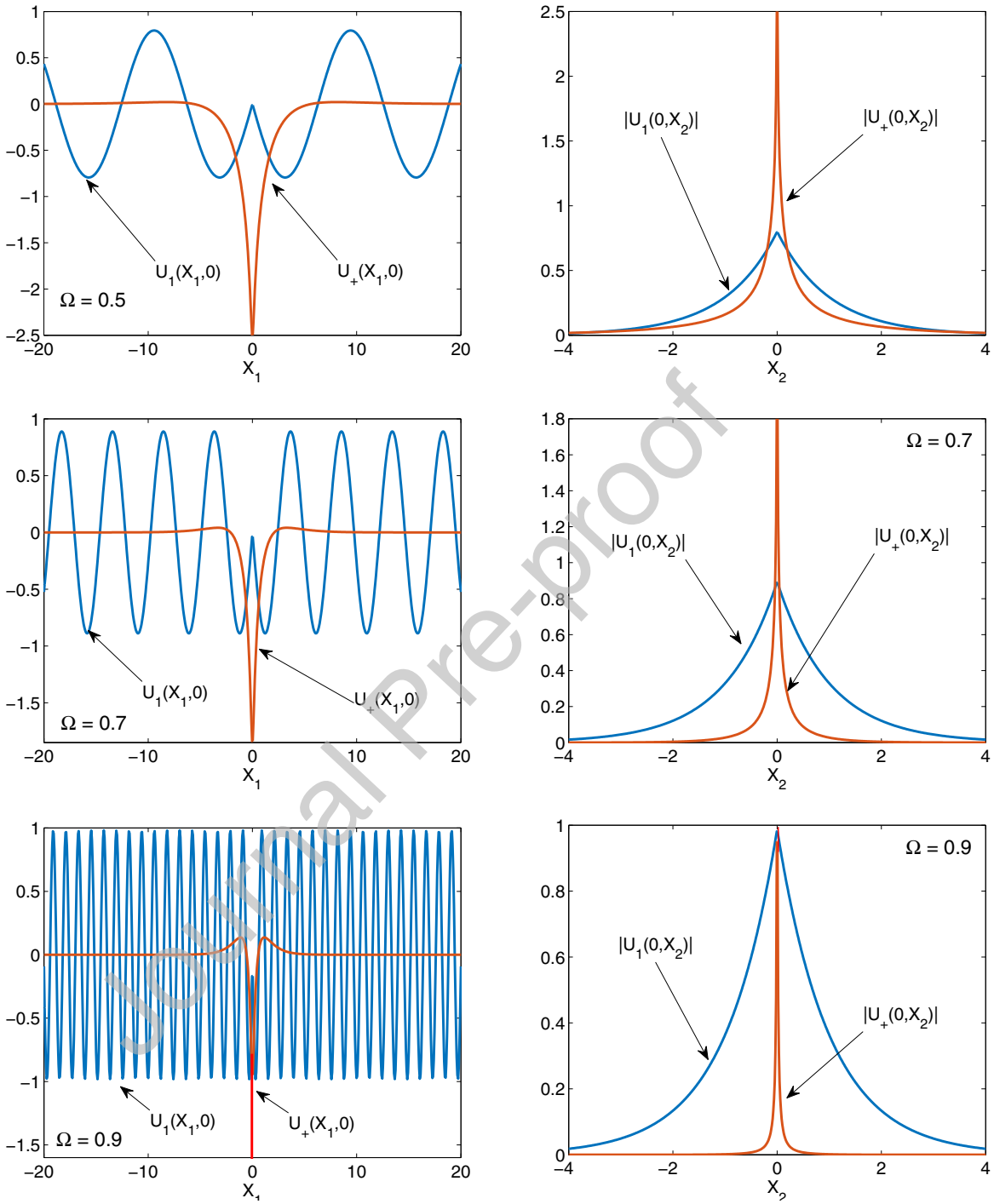

Figure 11: The dynamic field produced by the point oscillating force in the structured membrane on an elastic foundation. The localized wave, $U_1(X_1, X_2)$ and the sum of the divergent wave and the oscillations, $U_+ = U_2(X_1, X_2) + U_3(X_1, X_2)$, are presented for three frequencies, Ω =0.5, 0.7 and 0.9 for $\Omega_m = 0.4$. The wave profiles at $x_2 = 0$ (left) and $x_1 = 0$ (right) are shown.

where Ω_m, β_0 and ψ are defined in (55) and (56). The energy flux ratio

$$N_L(\Omega) = \frac{N_{1in}}{N_{tot}} = \left[1 + \frac{1}{2}\left(\sqrt{\frac{\Omega^2 - \Omega_m^2}{\psi^2} + \mathcal{R}^2(\Omega)} - \mathcal{R}(\Omega)\right)\right]^{-1} \quad (\Omega^2 > \Omega_m^2)\,, \tag{71}$$

with $N_L(\Omega) = 1 \quad (\Omega^2 < \Omega_m^2)$, $N_{tot} = N_{1in} + N_{2in}$. The ratio $N_L(\Omega)$ is plotted in Fig. 12.

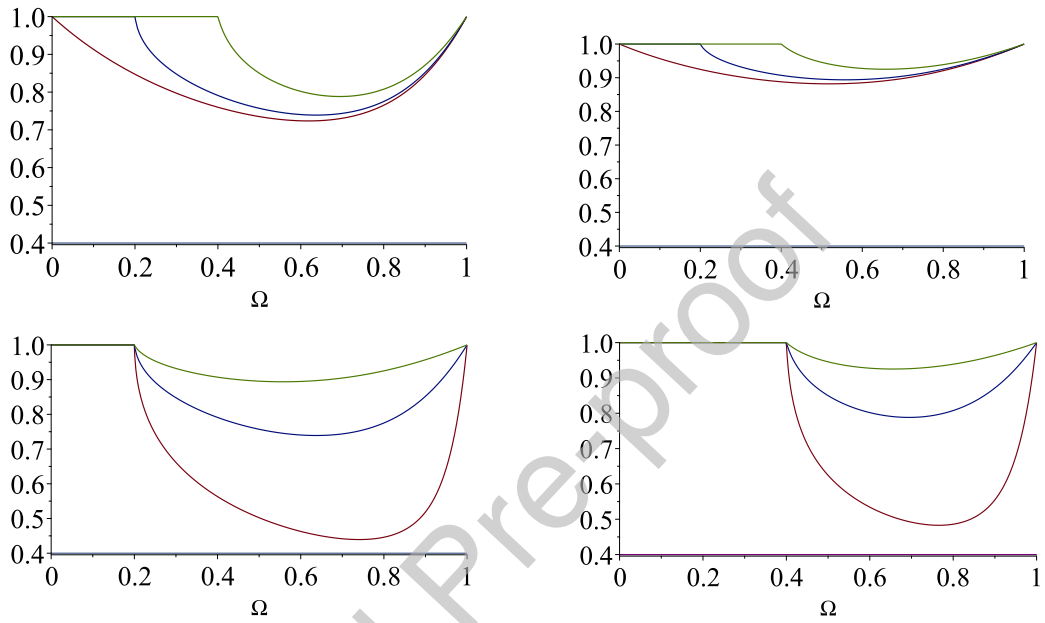

Figure 12: The energy flux ratio, $N_L = N_{1in}/N_{tot}$. For $\psi = 0.5$ (top, left) and $\psi = 1$ (top right) the curves correspond to $\Omega_m = 0, 0.2, 0.4$ (bottom to top, respectively). For $\Omega_m = 0.2$ (bottom, left) and $\Omega_m = 0.4$ (bottom, right) the curves correspond to $\psi = 0.2, 0.5, 1, 2$ (bottom to top, respectively).

In these graphs, the normalised global energy fluxes are presented, in the localized wave, N_L, and in the divergent wave, $1 - N_L$. Along with this, there exist local energy redistributions due to interactions of the propagating waves with the oscillations $u_3 = U_3 \exp(\mathrm{i}\omega t)$ (the latter is not orthogonal in energy to the former). In this sense, the u_3-oscillations play the role of a catalyst.

Remarkable, along with the wave localization, the structure decreases the bang gap width. The upper bound of it, Ω_{min}, corresponding to zero of K_{**} (58), appears lower than for the free membrane on the elastic foundation, Ω_m. Some plots of the ratio $\Lambda = \Omega_{min}/\Omega_m$ is presented in Fig. 13.

5 Concluding remarks

For sinusoidal waves of any nature, we have discussed the conditions under which the wave exponentially localizes at an inhomogeneity distributed on a line. In the application to solids,

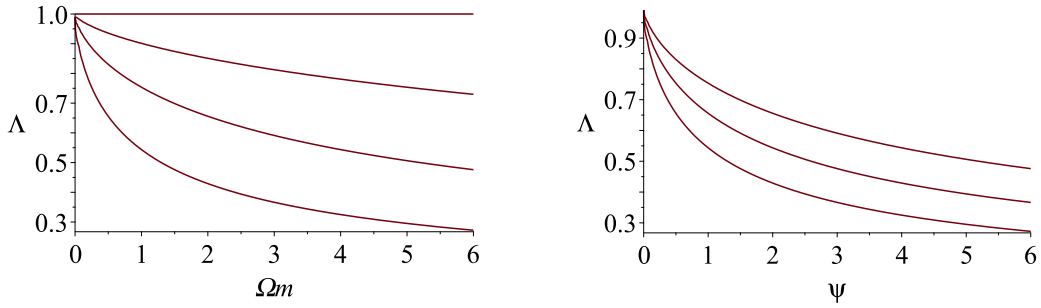

Figure 13: The ratio of the band gap width for the localized wave to that for a homogeneous membrane on an elastic foundation, $\Lambda = \Omega_{min}/\Omega_m$ ($K_{**} = 0$ at $\Omega = \Omega_{min}$). The curves correspond to $\psi = 0, 0.1, 0.5, 2$ (left, top down, respectively) and $\Omega_m = 0.5, 1, 2$ (right, top down, respectively).

line-distributed masses (possibly frequency-dependent) place the role of such an inhomogeneity. We note that the localization also occurs in an increased-inertia strip or a cylindrical area in a 3D body. In this case, the waveguide sizes correspond to those of the modified domains.

The frequency-domain where the localization is possible is bounded by resonance points, in the crossing of which the effective mass becomes negative. In connection with this, we note that in addition to the dynamic structure, such critical points can correspond to uniform structures too. Lattices and homogeneous bodies with discrete structures are examples. The role of such critical points becomes more pronounced as two or more resonant points coincide.

In more detail, we have considered free waves in the three different bodies structured by line-localized oscillators: a homogeneous elastic plate, a membrane with and without wave dispersion, respectively, and the discrete lattice. In these examples, the manifestation of the general localization conditions is illustrated, and different associated particulars are discussed.

The oscillators represent a frequency-dependent mass, and the latter grows unboundedly as the frequency approaches (from below) the oscillator's frequency. As a result, the localization is as strong as the frequency is close to the critical value.

We have shown that while the only localized free wave as the free one exists in such a structured system, the wave field produced by an oscillation force consists of three different parts: the localized wave, the divergent wave, and non-spread oscillations.

We believe that all these, the general statements and specific facts, can serve to better understanding the causes and effects in the subject area. In turn, this could facilitate the dealing with natural localization phenomena and the design of corresponding devices and materials with a (dynamic) microstructure.

Acknowledgements. ABM would like to acknowledge the support of the EPSRC Program grant EP/L024926/1. GM acknowledges financial support from the ERC Advanced Grant "Instabilities and nonlocal multiscale modelling of materials", ERC-2013-ADG-340561-INSTABILITIES. GM is also thankful to the Royal Society for the Wolfson Research Merit Award.

GM and LS are thankful to the Isaac Newton Institute for Mathematical Sciences, Cambridge, for Simon's Fellowship. All authors also would like to thank the Isaac Newton Institute for the support and hospitality during the programme "Bringing pure and applied analysis together via the Wiener-Hopf technique, its generalisations and applications" where work on this paper was mainly completed. The programme was supported by EPSRC grant EP/R014604/1.

References

Adams, S.D.M, Craster, R.V., and Williams, D.P., 2007. Rayleigh waves guided by topography. Proc. Roy. Soc. A. **463**, 531-550.

Babich, V.M., and Bilyi, I.Ya., 1979. Wave-guide properties of an underwater ridge. Fluid dynamics **14** (3), 449451.

Barros, A.C., and Gendron, P.J., 2019. A computational Bayesian approach for localizing an acoustic scatterer in a stratified ocean environment. The Journal of the Acoustical Society of America **146** (3), EL245-EL250.

Biot, M.A., 1937. Bending of an Infinite Beam on an Elastic Foundation. Journal of Applied Physics **12**, 155-164.

Evans, D.V., and Porter, R., 2007. Penetration of flexural waves through a periodically constrained thin elastic plate in vacuo and floating on water. Journal of Engineering Mathematics **58** (14), 317337.

Fu, Y.B., Rogerson, G.A., and Wang, W.F., 2013. Surface waves guided by topography in an anisotropic elastic half-space. Proc R Soc A **469**: 20120371.

Garipov, R.M., 1965. Nonsteady waves above an underwater ridge. Sov.Phys.Dokl. **10**, 194-196.

Haslinger, S. G., Movchan, N. V., Movchan, A. B., and Jones, I. S., 2015. Dynamic interfacial trapping of flexural waves in structured plates. arXiv:1509.05367v1 [math.AP] 17 Sep 2015.

Haslinger, S. G., Movchan, N. V., Movchan, A. B., Jones, I. S., and Craster, R. V., 2017. Controlling Flexural Waves in Semi-Infinite Platonic Crystals with Resonator-Type Scatterers. The Quarterly Journal of Mechanics and Applied Mathematics **70** (3), 216247.

Larose, E, Margerin, L, Van Tiggelen, B.A., and Campillo, M, 2004. Weak localization of seismic waves. Physical review letters **93** (4), 048501- 4.

Mandelshtam, L. I., 1972. Lectures of Optics, Theory of Relativity and Quantum Mechanics. Nauka, Moscow (in Russian).

Milton, G.W., and Willis, J.R., 2007. On modifications of Newton's second law and linear continuum elastodynamics. Proc. R. Soc. A **463**, 855880.

Mishuris, S., Movchan, A.B., and Slepyan, L.I., 2019. Waves in elastic bodies with discrete and continuous dynamic microstructure. Phil. Trans. R. Soc. A **378**: 20190313.

Munk, W.H.,1974. Sound channel in an exponentially stratified ocean, with application to SOFAR. The Journal of the Acoustical Society of America **55**, 220.

Kaina, N., Causier, A., Bourlier, Y., Fink, M., Berthelot, T., and Lerosey, G., 2017. Slow waves in locally resonant metamaterials line defect waveguides. Scientific Reports **7**, 15105.

Porter, R., 2019. An extended linear shallow-water equation. Journal of Fluid Mechanics **876**, 413-427.

Slepyan, L.I., 1967. The Strain Wave in a Bar with Vibration-Isolated Masses. Mechanics of Solids **2**, 57-64.

Slepyan, L.I., 1972. Nonstationary Elastic Waves. Sudostroenie, Leningrad (in Russian).

Slepyan, L.I., 2002. Models and Phenomena in Fracture Mechanics. Springer, Berlin.

Slepyan, L.I., 2018. Structural discontinuity as generalized strain and Fourier transform for discrete-continuous systems. Int. J. Engineering Sciences **130**, 199214.

Slepyan, L.I., 2019. About some projects with attendant circumstances. Phil. Trans. R. Soc. A **377**: 20190097.

Sobolev, S.L., 1937. Some questions of the propagation theory of oscillations. In: Frank, F. and Mizes, P. Differential and integral equations of mathematical physics. L. − M. ONTI (in Russian).

Author Statement

The paper presents new original results, which have been not published elsewhere. The revised version is submitted for publication in JMPS. Leonid Slepyan Professor Emeritus

Conflict of Interest

The authors declare that they have no known competing financial interests or personal relationships that could have appeared to influence the work reported in this paper.